Battery Charging Profile-Based Parameter Design of A 6.78-MHz Class E^2 Wireless Charging System

Ming Liu, *Student Member*, *IEEE*, Chen Zhao, Jibin Song, *Student Member*, *IEEE*, and Chengbin Ma, *Member*, *IEEE*

***Abstract*—Wireless power transfer (WPT) working at several megahertz (MHz), 6.78 or 13.56 MHz, is widely considered to be a promising candidate for charging electronic devices. The so-called Class E^2 converter combining the soft-switching based Class E power amplifier (PA) and Class E rectifier are known to be suitable for high-frequency applications with improved efficiency. However, the charging of batteries usually need to follow a specific profile, in which battery voltage and charging current vary over time. The input reactance of the Class E rectifier also becomes obvious at MHz. This non-neglectable and varying reactance significantly lowers system efficiency and complicates parameter design. In this paper, a systematic design approach is developed that minimizes the energy loss of a 6.78-MHz Class E^2 wireless charging system during the entire battery charging cycle. A LC matching network is added to improve the loading conditions of the Class E PA and coupling coils, and provide new degrees of freedom in the parameter design. Average power loss is defined based on analytically derived system efficiency and a discretized battery charging profile. It serves as an objective function that is minimized through the proposed battery charging profile-based parameter design. In final experiments, the proposed design achieves a 24.5% reduction of the average power loss when comparing with that through the conventional design.**

***Index Terms*—Battery charging system, charging profile, efficiency, lithium-ion battery, megahertz wireless power transfer.**

I. Introduction

In recent years, wireless power transfer (WPT) through inductive resonance coupling became popular to charge various electronic devices (e.g., cellphones, laptop computers, wearable devices, medical implant devices) and even electric vehicles [1], [2]. For high-power applications, WPT working at kilohertz (kHz) is making rapid progress in terms of coil design, compensation topologies, control strategies, etc. [3]–[6]. At the same time, in order to reduce size and weight of WPT systems, it is preferred to further increase the operating frequency to several megahertz (MHz) such as 6.78 and 13.56 MHz. A higher operating frequency also helps to improve spatial freedom, namely a longer transfer distance and higher tolerance to coupling coil misalignment, which is particularly beneficial for charging mobile devices. However, the power capability of the present switching devices is insufficient when operating at MHz. At present the MHz WPT is usually considered to be suitable for mid-range and low-power applications [2], [7]–[9].

A practical challenge for the MHz WPT is the high switching loss when using conventional hard-switching-based power amplifiers (PAs) and rectifiers. Class E PA and rectifier are promising candidates to build high-efficiency MHz WPT systems because of their soft-switching properties. The Class E PA was first introduced for high-frequency applications in [10]. It has been applied in MHz WPT systems and shown improvements thanks to its high efficiency and simple topology [11]–[14]. Similarly, the Class E rectifier has also been proposed for high-frequency rectification [15]. Its application in WPT was first investigated in [16]. A high efficiency of the rectifier, 94.43%, was reported at an 800 kHz operating frequency. Thus the combination of both Class E PA and rectifier, i.e., a Class E^2 converter, is expected to enable a high-efficiency wireless charging system working at MHz.

Lithium-ion batteries are now widely used in consumer electronic devices mostly due to its high energy density [17], [18]. A typical charging profile of the lithium-ion batteries usually consists of two modes, constant current (CC) mode and constant voltage (CV) mode. The battery is first charged in CC mode. When its voltage reaches a nominal value, the charging system enters the CV mode, in which the charging current rapidly drops. In order to prolong the battery cycle-life, a wireless charging system must supply current and voltage accurately following a specific battery charging profile [19]. In real applications, the charging profiles can be tracked through either the input voltage control of the charging system or the regulation circuit between the charger and batteries.

In the conventional Class E^2 converter for WPT applica-

Manuscript received Sep. 01, 2016; revised Dec. 30, 2016; accepted Jan. 29, 2017. This work was supported by the Shanghai Natural Science Foundation under Grant 16ZR1416300.

M. Liu, J. Song, and C. Ma are with the University of Michigan-Shanghai Jiao Tong University Joint Institute, Shanghai Jiao Tong University, Minhang, Shanghai 200240, China (e-mail: mikeliu@sjtu.edu.cn; jibinsong@sjtu.edu.cn; chbma@sjtu.edu.cn). C. Zhao is with United Automotive Electronic Systems Co., Ltd, Pudong, Shanghai 201206, China (e-mail: chen.zhao3@uaes.com).

tions, the system parameters are optimized targeting on only a single specific operating condition, i.e., fixed coil relative position and final load [20]. However, different with the conventional constant resistive loads, the battery voltage and current vary when following a charging profile. In addition, the input reactance of the Class E rectifier is non-neglectable at MHz and changes with the varying battery voltage and current. This obvious and varying input reactance of the Class E rectifier increases the power loss and complicates the design of a high-efficiency MHz Class E^2 wireless battery charging system. In KHz wireless charging systems, compensation networks (such as a LLC network) and designs have been discussed to achieve a load-variation-independent resonant frequency [5]. However, these existing approaches are not valid anymore for the MHz Class E^2 wireless battery charging systems due to the non-neglectable and varying input reactance of the Class E rectifier.

This paper proposes a systematic and general parameter design approach that achieves a high-efficiency Class E^2 MHz wireless battery charging system. The influence of the non-neglectable input reactance of the Class E rectifier is first analyzed when working at 6.78 MHz and following a battery charging profile. This aspect is quite different with the KHz WPT systems, in which the input impedance of the rectifier is pure resistive. A LC matching network is added that works with the series compensation capacitor of the receiving coil to mitigate the influence of the non-neglectable and varying input reactance of the rectifier. The LC matching network also provides new degrees of freedom in the following parameter design. In order to minimize the energy loss of the MHz Class E^2 wireless battery charging system during the entire charging cycle, average power loss is defined and calculated based on a discretized battery charging profile and analytically derived system efficiency. This average power loss is used as the objective function in the following optimization of the system design parameters. Finally, both the analytical derivations and design optimization are validated in experiments.

II. Preliminary Analysis

The configuration of a classical 6.78-MHz Class E^2 wireless battery charging system is shown in Fig. 1. It consists of the Class E PA, coupling coils, Class E rectifier, and lithium-ion batteries. L_{tx} and L_{rx} represent the transmitting and receiving coils, respectively; r_{tx} and r_{rx} are equivalent series resistance (ESR) of L_{tx} and L_{rx}; C_{tx} and C_{rx} are compensation capacitors; Z_{in} is the input impedance of the coupling coils, and Z_{out} is the input impedance seen from the receiving coil; V_{bat} and I_{bat} are the battery voltage and charging current, respectively.

The typical charging profile of a lithium-ion battery usually consists of two modes, constant current (CC) mode and constant voltage (CV) mode. The wireless battery charging system is expected to provide accurate charging current and voltage that well follow the desired charging profile. Fig. 2 shows an example charging profile of a lithium-ion battery pack with four SANYO UR18650A batteries included (4S1P, 4 series 1 parallel). This battery pack is used in the final

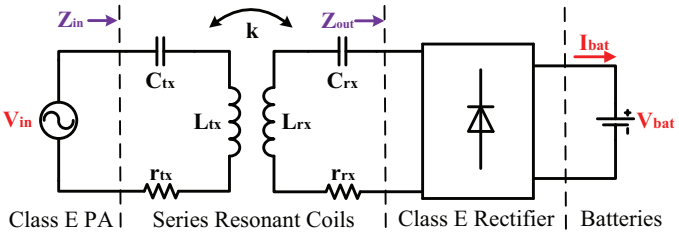

Fig. 1. The configuration of a classical 6.78-MHz Class E^2 wireless battery charging system.

experiments, section V. In this charging profile, the constant charging current is 1 A and the constant battery voltage is 16.8 V, i.e., the nominal charging current and voltage, I_{bat}^{nom} and V_{bat}^{nom}. The varying charging voltage and current will influence the values of Z_{out} and Z_{in}, and thus negatively affect the efficiencies of the coupling coil and Class E PA, as discussed below. Their influences become obvious in the MHz Class E^2 wireless charging systems due to the highly nonlinear behavior of the Class E rectifier when working at MHz.

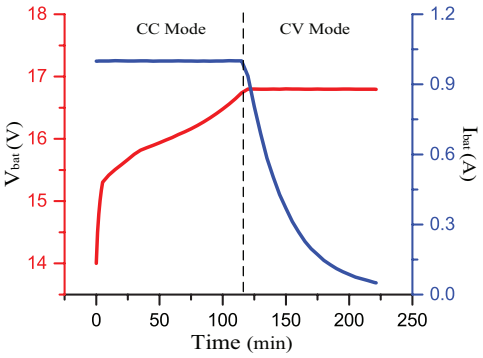

Fig. 2. The charging profile of the SANYO UR18650A lithium-ion battery pack.

TABLE I
Parameters of Coupling Coils.

k	L_{tx}	L_{rx}	C_{tx}	C_{rx}	r_{tx}	r_{rx}
0.2	3.34 μH	3.34 μH	165 pF	165 pF	0.7 Ω	0.7 Ω

The performance of the above 6.78-MHz Class E^2 wireless battery charging system in Fig. 1 is investigated using a well-known nonlinear radio-frequency (RF) circuit simulation software, advanced design system (ADS) from Keysight. The parameters of the coupling coils are given in Table I. In the simulation, a half-wave Class E rectifier is employed. The same Class E rectifier is used in the following analysis and experiments. Fig. 3(a) shows the simulation results of the resistance and reactance of Z_{out}, R_{out} and X_{out}, under the charging profile given in Fig. 2. The capacitive, i.e., negative, reactance X_{out} dramatically increases in the CV mode. This large reactance significantly affects the efficiency and thus power transfer capability of the coupling coils, as shown in Fig. 3(b). Fig. 4 gives the simulation results of the input impedance of the coupling coils. Due to the increasing X_{out}, the resistance and reactance of Z_{in}, R_{in} and X_{in}, decrease

rapidly in the CV mode. The small resistance of Z_{in} will lead to the high power loss on the self-resistance of L_{tx}, r_{tx}, and parasitic resistances of the components in the Class E PA. In addition, the varying R_{in} and X_{in}, i.e., the load of the PA, may negatively affect the ZVS operation of the highly load-sensitive Class E PA.

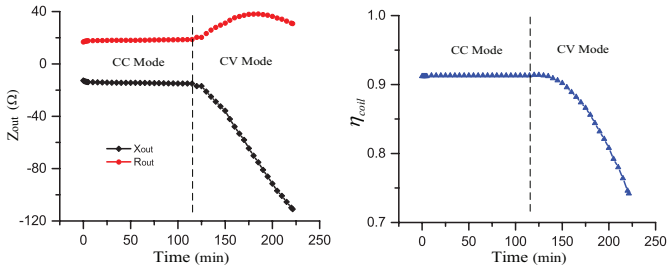

Fig. 3. Simulation results of the input impedance seen from the receiving coil and efficiency of the coupling coils. (a) Z_{out}. (b) η_{coil}.

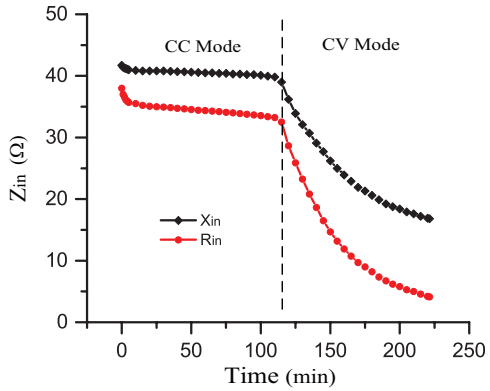

Fig. 4. Simulation results of the input impedance of the coupling coils Z_{in}.

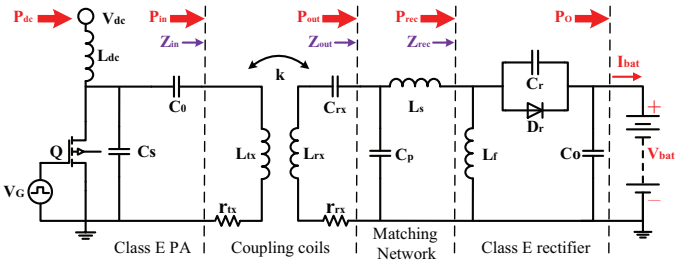

Fig. 5. Circuit topology of the proposed 6.78-MHz Class E^2 wireless battery charging system.

As discussed above, following a required battery charging profile leads to a changing impedance characteristics, and thus significantly affects the efficiencies of the coupling coil and Class E PA when operating at MHz. It complicates the design and implementation of high-efficiency MHz Class E^2 wireless charging systems. In order to mitigate the influences of the changing battery charing current and voltage, a LC matching network (MN) can be added into the classical Class E^2 wireless charging system. As shown in Fig. 5, the matching network locates between the coupling coils and Class E rectifier. It improves the loading conditions of the coupling coils and Class E PA, and introduces new degrees of design freedom that optimize the overall system efficiency under the battery charging profile. In Fig. 5, the compensation capacitor of the transmitting coil, C_{tx}, is absorbed into the series capacitor of the Class E PA, C_0. L_{dc} and L_f are the dc filter inductors of the Class E PA and rectifier, respectively. C_s is the parallel capacitors of the Class E PA. C_r and C_o are the shunt capacitor and dc output capacitor of the Class E rectifier. L_s and C_p are the series inductor and parallel capacitor of the LC network, respectively.

III. Efficiency Derivation

The equivalent circuit model of the proposed 6.78-MHz Class E^2 wireless battery charging system is given in Fig. 6. This circuit model facilitates the following derivation of the system efficiency. In the circuit model, the two dc filter inductors, L_{dc} and L_f, are represented by their equivalent series resistances (ESRs) $r_{L_{dc}}$ and r_{L_f}, respectively. The ac inductor of the LC matching network is modeled as a series combination of its inductance L_s and ESR r_{L_s}. Table II summarizes the definitions of all the circuit parameters. Z_{out} is the input impedance seen by the receiving coil, and Z_{in} is the input impedance of the coupling coils. R_{dc} is the equivalent resistance of the entire charging system seen by the dc power supply. I_{dc} and I_{bat} are the dc input and output currents of the charging system. i_{in} and i_{out} are the sinusoidal input and output currents of the coupling coils. i_{rec} is the sinusoidal input current of the Class E rectifier. i_Q is the switch current when Q is on. Similarly i_{D_r} is the current that flows through the diode when D_r is on. P_{in} and P_{out} are the input and output powers of the coupling coil. P_{rec} is the input power of the rectifier.

TABLE II
Circuit Parameters

Parameter	Definition
$r_{L_{dc}}$	ESR of dc filter L_{dc}
r_Q	on-resistance of MOSFET Q
C_S	shunt capacitor of PA
C_0	series capacitor of PA
L_{tx}	inductance of transmitting coil
r_{tx}	ESR of transmitting coil
L_{rx}	inductance of receiving coil
r_{rx}	ESR of receiving coil
L_m	mutual inductance
C_p	parallel capacitor of MN
L_s	series inductor of MN
r_{L_s}	ESR of ac filter L_s
r_{L_f}	ESR of dc filter L_f
C_r	parallel capacitor of rectifier
V_f	diode forward voltage drop
r_{D_r}	on-resistance of diode
C_o	dc output filter

According to [21], the equations for the Class E rectifier that involve in the following efficiency derivation can be

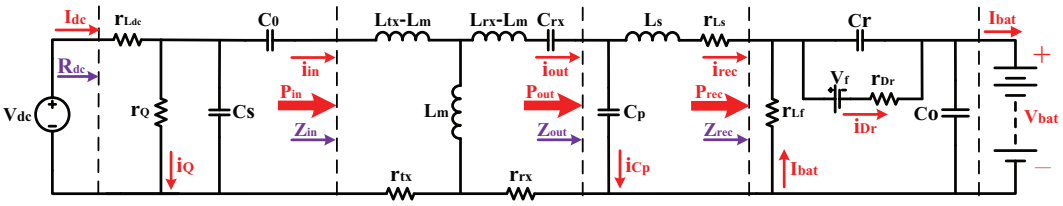

Fig. 6. Equivalent circuit model of the proposed 6.78-MHz Class E^2 wireless battery charging system.

obtained,

$$I_{m,rec} = -\frac{I_{bat}}{\sin\phi_1}, \tag{1}$$

$$\tan\phi_1 = \frac{1-\cos 2\pi D}{\sin 2\pi D + 2\pi(1-D)}, \tag{2}$$

$$\frac{2\pi\omega V_{bat}C_r}{I_{bat}} = 1 + \frac{[\sin 2\pi D + 2\pi(1-D)]^2}{1-\cos 2\pi D} - 2\pi^2(1-D)^2 - \cos 2\pi D, \tag{3}$$

and

$$R_{rec} = \frac{2V_{bat}\sin^2\phi_1}{I_{bat}}, \tag{4}$$

$$X_{rec} = -\frac{1}{\pi}\left[\frac{a+b}{\omega C_r}\right], \tag{5}$$

$$a = \pi(1-D) + 2\pi(1-D)\sin\phi_1\sin(\phi_1 - 2\pi D), \tag{6}$$

$$b = \sin 2\pi D + \frac{1}{4}\sin(2\phi_1 - 4\pi D) - \frac{1}{4}\sin 2\phi_1, \tag{7}$$

where ϕ_1 is the initial phase of i_{rec}; D is the duty cycle of the rectifying diode; ω is the operating frequency, 6.78-MHz here; R_{rec} and X_{rec} are the resistance and reactance of Z_{rec}; $I_{m,rec}$ is the amplitude of i_{rec}; a and b are the intermediate variables.

As shown in Fig. 6, the below relationship exists,

$$P_{out} = P_{rec} + P_{L_s,loss}, \tag{8}$$

where $P_{L_s,loss}$ is the power loss on L_s. Because i_{out} and i_{rec} are sinusoidal, the above equation can be rewritten as

$$I_{m,out}^2 R_{out} = I_{m,rec}^2 R_{rec} + I_{m,rec}^2 r_{L_s}, \tag{9}$$

where $I_{m,out}$ is the amplitude of i_{out} and R_{out} is the resistance of the input impedance seen by the receiving coil, Z_{out}. From the circuit model in Fig. 6, $Z_{out}(= R_{out} + jX_{out})$ can be derived as

$$R_{out} = \frac{R_{rec}+r_{L_s}}{(\omega C_p)^2[(R_{rec}+r_{L_s})^2+(\frac{1}{\omega C_p}+\omega L_s+X_{rec})^2]}, \tag{10}$$

$$X_{out} = \frac{(\omega C_p)(R_{rec}+r_{L_s})^2+(X_{rec}+\omega L_s)}{(\omega C_p)^2[(R_{rec}+r_{L_s})^2+(\frac{1}{\omega C_p}+\omega L_s+X_{rec})^2]}. \tag{11}$$

Substituting (1) into (9) gives

$$I_{m,out} = \frac{I_{bat}}{|\sin\phi_1|}\sqrt{\frac{R_{rec}+r_{L_s}}{R_{out}}}. \tag{12}$$

Similarly,

$$I_{m,in}^2 R_{in} = I_{m,in}^2 r_{tx} + I_{m,out}^2 r_{rx} + I_{m,out}^2 R_{out}, \tag{13}$$

where $I_{m,in}$ is the amplitude of i_{in} and R_{in} is the resistance of the input impedance of the coupling coils, Z_{in}. Thus

$$I_{m,in} = \frac{I_{bat}}{|\sin\phi_1|}\sqrt{\frac{R_{rec}+r_{Ls}}{R_{out}}}\sqrt{\frac{R_{out}+r_{rx}}{R_{in}-r_{tx}}}. \tag{14}$$

Again, from the circuit model, $Z_{in}(= R_{in} + jX_{in})$ can be derived as follows,

$$R_{in} = r_{tx} + \frac{\omega^2 {L_m}^2(R_{out}+r_{rx})}{(R_{out}+r_{rx})^2 + (X_{out}+\omega L_{rx} - \frac{1}{\omega C_{rx}})^2}, \tag{15}$$

$$X_{in} = \omega L_{tx} - \frac{\omega^2 {L_m}^2(X_{out}+\omega L_{rx} - \frac{1}{\omega C_{rx}})}{(R_{out}+r_{rx})^2 + (X_{out}+\omega L_{rx} - \frac{1}{\omega C_{rx}})^2}. \tag{16}$$

In the above equations, L_m is the mutual inductance,

$$L_m = k\sqrt{L_{tx}L_{rx}}, \tag{17}$$

where k is the mutual inductance coefficient. The dc input current and equivalent resistance of the wireless charging system can be obtained as follows [22],

$$I_{dc} = \frac{I_{m,in}}{g}, \tag{18}$$

$$R_{dc} = \frac{\pi^2 - g(2\pi\cos\phi_2 + 4\sin\phi_2)}{4\pi\omega C_S}, \tag{19}$$

where

$$g = \frac{2\pi\sin(\varphi+\phi_2) + 4cos(\varphi+\phi_2)}{4\cos\phi_2\sin(\varphi+\phi_2) + \pi\cos\varphi}, \tag{20}$$

$$\varphi = \arctan\frac{X_{in} - \frac{1}{\omega C_0}}{R_{in}}, \tag{21}$$

$$\phi_2 = \arctan\frac{\frac{\pi^2}{2} - 4 - \pi\omega C_S\left[2R_{in} + \pi(X_{in} - \frac{1}{\omega C_0})\right]}{\pi + \pi^2\omega C_S R_{in} - 2\pi\omega C_S(X_{in} - \frac{1}{\omega C_0})}. \tag{22}$$

ϕ_2 is initial phase of i_{in}; g and φ are the intermediate variables. Substituting (14) into (18) gives

$$I_{dc} = \frac{I_{bat}}{g\,|\sin\phi_1|}\sqrt{\frac{R_{rec}+r_{Ls}}{R_{out}}}\sqrt{\frac{R_{out}+r_{rx}}{R_{in}-r_{tx}}}. \tag{23}$$

There are also power losses from the two dc filter inductors, L_{dc} and L_f, switch Q and diode D_r. Thus the overall system efficiency is expressed as below,

$$\eta_{sys} = \frac{I_{bat}V_{bat}}{I_{dc}^2 R_{dc} + I_{dc}^2 r_{L_{dc}} + I_{bat}^2 r_{L_f} + P_{Q,loss} + P_{D_r,loss}}, \tag{24}$$

$$\eta_{sys} = \frac{4\pi V_{bat}}{\frac{I_{bat}[(R_{rec}+r_{Ls})(R_{out}+r_{rx})]\left[4\pi(R_{dc}+r_{L_{dc}})+(2\pi+8\cos\phi_2 g+\pi g^2)r_Q\right]}{R_{out}(R_{in}-r_{tx})g^2\sin^2\phi_1} + 4\pi\left[I_{bat}(r_{L_f}+er_{D_r})+fV_f\right]}. \quad (29)$$

where

$$P_{Q,loss} = \frac{1}{2\pi}\int_0^{\pi} i_Q^2 r_Q d\omega t = \left(\frac{1}{2} + 2\cos\phi_2\frac{g}{\pi} + \frac{g^2}{4}\right) I_{dc}^2 r_Q, \quad (25)$$

$$P_{D_r,loss} = \frac{1}{2\pi}\int_0^{2\pi D} (i_{D_r}^2 r_{D_r} + i_{D_r} V_f) d\omega t = eI_{bat}^2 r_{D_r} + fI_{bat}V_f. \quad (26)$$

The coefficients are

$$f = 2\pi + \cot\phi_1 - \frac{\cos(\phi_1 - 2\pi D)}{\sin\phi_1}, \quad (27)$$

$$e = D + \frac{D}{2\sin^2\phi_1} - \frac{\cos(\phi_1 - 2\pi D)}{\pi\sin\phi_1} + \frac{3\sin 2\phi_1 + \sin(2\phi_1 - 4\pi D)}{8\pi\sin^2\phi_1}. \quad (28)$$

Substituting (23)(25)(26) into (24) gives (29), the overall efficiency of the wireless charging system, η_{sys}. It can be seen that η_{sys} depends on the battery voltage V_{bat}, charging current I_{bat}, parasitic parameters of the components, and system parameters. Note that the influences of the system parameters are represented by R_{dc}, R_{in}, R_{out}, and R_{rec} in (29).

As discussed in section II, when operating at MHz, following the battery charging profile leads to a varying battery voltage (V_{bat}) and charging current (I_{bat}), and thus a large and varying input reactance of the Class E rectifier (X_{rec}). It will not only negatively affect the efficiency of the wireless charging system but also present challenges in the optimized design of the system. A systematic parameter design approach is developed below that minimizes the energy loss of the MHz Class E^2 wireless battery charging system over the entire charging cycle.

IV. Design Parameters Optimization

At given time t in the battery charging profile, the output power of the charging system, P_o, is

$$P_o(t) = I_{bat}(t)V_{bat}(t). \quad (30)$$

Then the total power loss, P_{loss}, at time t is

$$P_{loss}(t) = \frac{P_o(t)}{\eta_{sys}(t)} - P_o(t) = \frac{I_{bat}(t)V_{bat}(t)}{\eta_{sys}(t)}\left[1 - \eta_{sys}(t)\right]. \quad (31)$$

Here $\eta_{sys}(t)$ can be calculated by substituting $I_{bat}(t)$ and $V_{bat}(t)$ into (29). For the following optimization, the charging profile is evenly divided into N pieces. Thus the average power loss based on the discretized battery charging profile, namely the objective function of the optimization problem, is defined as

$$P_{loss}^{avg} = \frac{\sum_{i=1}^{N}\frac{I_{bat}(t_i)V_{bat}(t_i)}{\eta_{sys}(t_i)}[1-\eta_{sys}(t_i)]}{N}. \quad (32)$$

As shown in Fig. 5, the purpose of the LC matching network is to improve the loading condition of the coupling coils. Thus the inductor L_s should be designed to partly compensate the non-neglectable reactance of the input impedance of the Class E rectifier operating at MHz. From (5),

$$L_s = -\frac{X_{rec}}{\omega}\bigg|_{V_{bat}^{nom},I_{bat}^{nom}} = \frac{1}{\pi}\left[\frac{a+b}{\omega^2 C_r}\right]\bigg|_{V_{bat}^{nom},I_{bat}^{nom}}, \quad (33)$$

which targets the nominal operating condition, i.e., the nominal battery voltage and charging current, V_{bat}^{nom} and I_{bat}^{nom}. Note that X_{rec} is determined by C_r, V_{bat}, and I_{bat} [refer to (3)(5)]. Then the ESR of L_s, r_{L_s}, can be calculated,

$$r_{L_s} = \frac{\omega L_s}{Q_{L_s}} = \frac{1}{\pi Q_{L_s}}\left[\frac{a+b}{\omega C_r}\right]\bigg|_{V_{bat}^{nom},I_{bat}^{nom}}, \quad (34)$$

where Q_{L_s} is the quality factor of L_s. Note that a candidate C_r is given for calculating L_s during the below design optimization.

The design parameters, the capacitors, in the below optimization are finalized as follows,

$$\mathbf{x} = [C_S, C_0, C_{rx}, C_p, C_r], \quad (35)$$

that minimizes the average power loss, P_{loss}^{avg} over the entire charging profile. Here $\mathbf{x}$ is a vector. C_S and C_0 are the parallel and series capacitors of the Class E PA; C_{rx} is the compensation capacitor of the receiving coil; C_p is the parallel capacitor of the LC matching network; and C_r is the shunt capacitor of the Class E rectifier. Again, due to the non-neglectable X_{rec}, C_{rx} is also taken as a design parameter that further lowers the influence of X_{rec} during the entire charing cycle. Thus, unlike in the conventional design, the resonance of the receiving coil is not pre-assumed here. The constant parameters in the proposed optimized design of the wireless charging system are

$$\mathbf{p_{con}} = [L_{tx}, L_{rx}, V_f, r_{D_r}, r_{tx}, r_{rx}, r_{L_{dc}}, r_{L_f}, r_Q, \omega, k]. \quad (36)$$

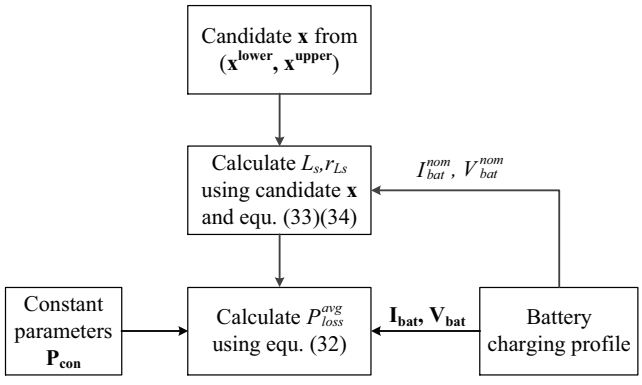

Fig. 7. Relationship between the constant and design parameters, and battery charging profile in the optimized design.

The design optimization problem is formulated as follows,

$$\min_{\mathbf{x}} P_{loss}^{avg}(\mathbf{x}, \mathbf{p_{con}}, \mathbf{I_{bat}}, \mathbf{V_{bat}}) \quad (37)$$

$$s.t.\ \mathbf{x} \in (\mathbf{x^{lower}}, \mathbf{x^{upper}}), \quad (38)$$

where $\mathbf{x^{lower}}$ and $\mathbf{x^{upper}}$ are the lower and upper feasible bounds of $\mathbf{x}$, respectively. $\mathbf{I_{bat}}$ and $\mathbf{V_{bat}}$ represent the discredited battery charging profile,

$$\mathbf{I_{bat}} = [I_{bat}(t_1), I_{bat}(t_2), \ldots, I_{bat}(t_N)], \quad (39)$$

$$\mathbf{V_{bat}} = [V_{bat}(t_1), V_{bat}(t_2), \ldots, V_{bat}(t_N)]. \quad (40)$$

The average power loss, P_{loss}^{avg}, is determined by the design and constant parameters of the MHz wireless charging system, and the specific battery charging profile [refer to (32) and Fig. 7]. The purpose of the optimization problem is to find an optimal set of the design parameters, $\mathbf{x_{opt}}$, that achieves the lowest average power loss over a specific charging profile. The proposed design optimization is a general solution that minimizes the energy loss when charging batteries with different profiles, i.e., different $\mathbf{I_{bat}}$ and $\mathbf{V_{bat}}$. Given the nature of the above optimization problem, it is appropriate to apply genetic algorithm (GA), a popular population-based heuristic approach, to locate a global or at least near-to-global optimal solution [23], [24].

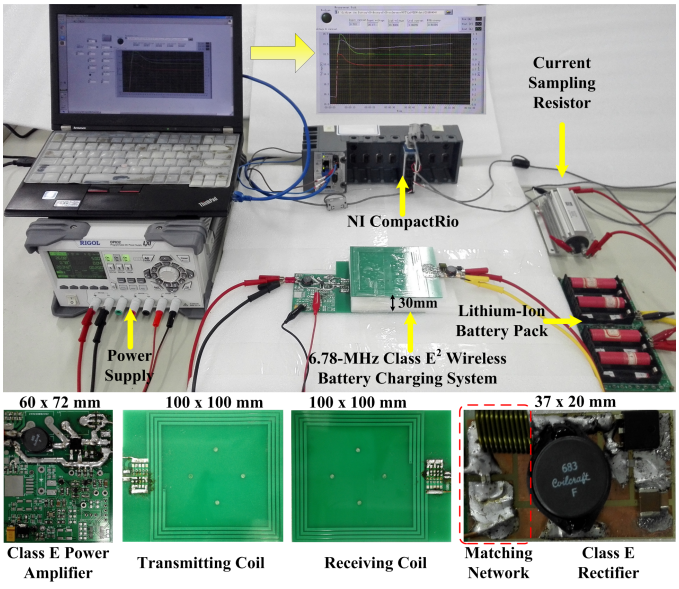

Fig. 8. Experimental setup of the proposed 6.78-MHz Class E^2 wireless battery charging system.

V. Experimental Results

As shown in Fig. 8, an experimental Class E^2 wireless charging system working at 6.78 MHz is built up to validate the above proposed configuration and parameter design. The lithium-ion battery pack uses four SANYO UR18650A batteries connected in 4S1P. In experiments, the battery charging profile in Fig. 2 is implemented through the control of the dc input voltage of the wireless charging system, i.e., the output voltage of the power supply. A high-accuracy sampling resistor is connected in series with the battery pack for charging current measurement. The National Instruments (NI) CompactRio system is employed to measure/sample the battery voltage and charging current, $V_{bat}(t)$ and $I_{bat}(t)$, and control the dc output voltage of the power supply based on the voltage and current feedback signals. In the CC mode, the power supply is controlled by the NI compactRIO system to increase its dc output voltage in order to achieve the constant battery charging current. Similarly, after the battery voltage reaches the nominal value, the power supply dc output voltage is decreased to keep the constant battery voltage, i.e., the CV mode. When the battery charging current is lower than the termination current (here 0.05 A recommended by the datasheet of the battery cell), the charging cycle stops. The wireless battery charging system has the same configuration as that in Fig. 5. Its constant parameters, $\mathbf{p_{con}}$, are summarized in Table III. The distance of the coupling coils is 30 mm corresponding to a mutual inductance coefficient, k=0.2. A MOSFET SUD06N10 and a silicon carbide diode STPSC406 are used as the switch Q and rectifying diode D_r of the Class E PA and rectifier, respectively. The parasitic capacitors of SUD06N10 and STPSC406 are assumed to be constant, 50 pF and 35 pF, according to their datasheets. Note that these two parasitic capacitances are included in the calculated final C_r and C_S, respectively.

TABLE III
Constant Parameters

ω	L_{tx}	L_{rx}	V_f	r_{D_r}	r_Q
6.78 MHz	3.34 μ H	3.34 μ H	1.2 V	0.3 Ω	0.225 Ω
k	r_{tx}	r_{rx}	$r_{L_{dc}}$	r_{L_f}	-
0.2	0.7 Ω	0.7 Ω	0.2 Ω	0.2 Ω	-

In the experiments, the feasible range of the design parameters, $\mathbf{x} = [C_S, C_0, C_{rx}, C_p, C_r]$, are given as

$$\mathbf{x^{lower}} = [100\text{ pF}, 100\text{ pF}, 100\text{ pF}, 100\text{ pF}, 100\text{ pF}],$$
$$\mathbf{x^{upper}} = [2000\text{ pF}, 2000\text{ pF}, 2000\text{ pF}, 2000\text{ pF}, 2000\text{ pF}] \quad (41)$$

Here the feasible ranges are estimated based on the inductances of the coupling coils and equivalent loads under the battery charging profile. By applying the design procedures developed in section IV and charging profile in Fig. 2, the optimal design parameters, $\mathbf{x_{opt}}$, and thus L_s, the inductor of the LC matching network, are calculated as follows,

$$\mathbf{x_{opt}} = [105\text{ pF}, 250\text{ pF}, 195\text{ pF}, 192\text{ pF}, 120\text{ pF}], \quad (42)$$

$$L_s = 323\text{ nH}. \quad (43)$$

The inductance of L_s is finalized as 330 nH, which is commercially available. In the above optimization, the total number of the sampling instants of the charging profile, N, is chosen as 50. There are 28 sampling instants in the CC mode, and 22 instants in the CV mode. Thus the system efficiency during the CC mode is particularly emphasized.

In the experiments, the battery charging profile is accurately followed by controlling the dc output voltage of the power supply V_{dc} (see Fig. 5). Fig. 9(a) and (b) show V_{dc} and P_o, the input voltage and output power of the experimental wireless charging system under the single charging profile in Fig. 2.

In the CC mode, the current is controlled as 1 A and the battery voltage increases until it reaches the nominal value 16.8 V at charge time t=115 min. After entering the CV mode, V_{dc} decreases rapidly in order to maintain the nominal battery voltage. The output power of the wireless charging system shows a similar trend.

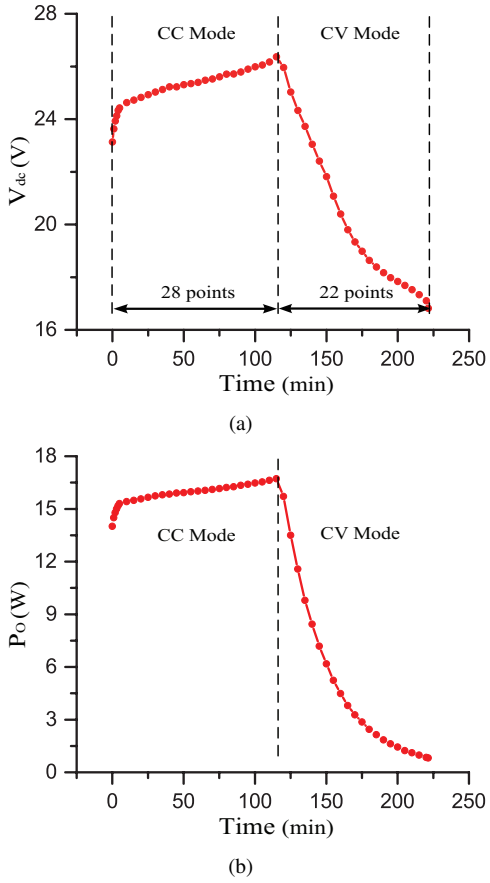

Fig. 9. The dc input voltage and output power of the experimental wireless charging system under a single charging profile. (a) V_{dc}. (b) P_o.

Fig. 10–12 compare the system and component-level efficiencies and overall power loss when applying the conventional and proposed designs. In the conventional design, the design parameters are optimized targeting on only a single operation condition, i.e., the nominal battery voltage and charging current, V_{bat}^{nom} and I_{bat}^{nom} [20]. The goals of the convectional design are 1) resonance of the receiving coil exactly at the target frequency, 6.78 MHz here; 2) ZVS operation of the Class E PA when its load, i.e., the input impedance of the coupling coil Z_{in}, is as equal as the one under V_{bat}^{nom} (= 16.8 V) and I_{bat}^{nom} (=1 A); 3) a duty cycle D (=0.5) of the rectifying diode, D_r, in the Class E rectifier, again, under V_{bat}^{nom} and I_{bat}^{nom} [21]. Its circuit model can be obtained by removing the LC matching network in Fig. 5. The results of the conventional design are calculated and listed in Table IV based on the constant parameters given in Table III and the nominal operating condition.

As shown in Fig. 10 and 11, the proposed design demonstrates obvious improvements in both system efficiency and power loss during the entire charging cycle. The experimental

TABLE IV
RESULTS OF CONVENTIONAL DESIGN

C_S	C_0	C_{rx}	C_r
130 pF	168 pF	165 pF	420 pF

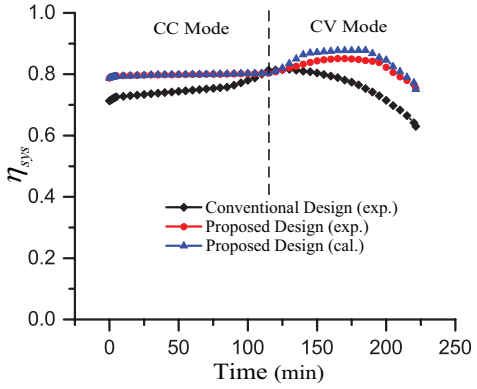

Fig. 10. Experimental results of the system efficiency.

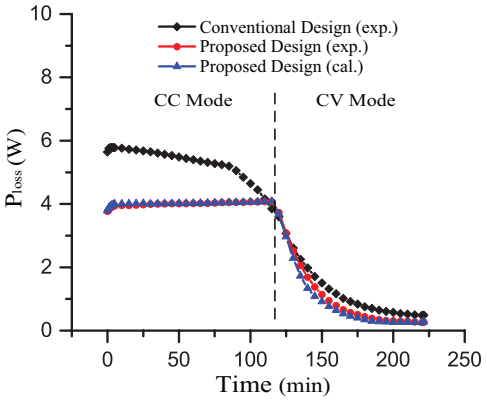

Fig. 11. Experimental results of the power loss.

results using the proposed design well match the calculated results, which verifies the correctness of the analytical derivations in section III. The conventional design achieves optimized performance only when the nominal operating condition, its design target, is met, i.e., V_{bat}^{nom}=16.8 V and I_{bat}^{nom}=1 A at t=115 min. When the operation deviates from this nominal one, its performance starts to deteriorate. The proposed design outpaces the conventional design within the most charging cycle because it is optimized targeting on the battery charging profile rather than a specific single operating condition.

Note that mostly due to improved coupling coil efficiency in the proposed parameter design, the final system efficiency when using the conventional design is not obviously higher (1.0% percentage improvement) even under the nominal operating condition [see Figs. 10 and 12]. In the conventional design, the design parameters are optimized with the given coupling coils and targeting on the nominal battery voltage and charging current, i.e., a specific fixed nominal load. However, this nominal load does not necessarily equal to the final load that corresponds to the highest achievable efficiency of the given coupling coils [25]. It is because practically coupling

coils are usually designed to first meet other requirements such as targeted size, transfer distance, and power level. Meanwhile, thanks to the LC matching network and proposed parameter design, the coupling coils work under a better loading condition (namely a load different with the one seen by the receiving coil in the conventional design), and thus with obviously improved efficiency. This aspect can be particularly explained by Fig. 12(a) and (b), the component-level efficiencies in the experiments. Since the efficiency of the Class E rectifier is largely determined by the battery voltage and charging current, its efficiencies in the two designs are close. Thus the efficiencies of the coupling coils (η_{coil}) and Class E PA (η_{pa}) are shown in the two subfigures. Besides the improved coupling coil efficiency, using the proposed design the Class E PA also demonstrates higher efficiency during the most high-power period (e.g., charging time from 0 to 105 min) [refer to Fig. 9(b)]. Note that the PA efficiency in the conventional design is higher when the operating condition is close to the nominal one, i.e., its design target, while the target of the proposed design is to minimize the energy loss over the entire charging cycle.

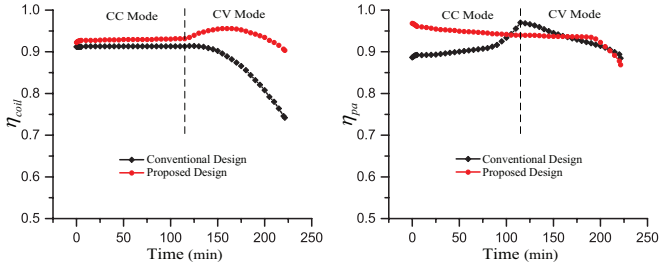

Fig. 12. Experimental results of the efficiencies of the coupling coils and Class E PA. (a) η_{coil}. (b) η_{pa}.

Table V lists the average power loss, P_{loss}^{avg}, and the total energy loss, E_{loss}, within the single battery charging profile. Here E_{loss} equals the production of P_{loss}^{avg} and total charging time, 221 minutes. With the proposed parameter design, the average power loss is reduced by 24.5% when comparing with that in the conventional design. The saved total energy is 11536 J. From the above experimental results, the average efficiencies of the conventional design and proposed design are 74.5% and 80.9%, respectively, namely 8.6% improvement percentage of the system efficiency over the entire charging cycle. Because the objective function in the optimization problem is the average power loss, (32), naturally the proposed design assigns higher priority to achieving higher efficiency during the high-power period. This leads to the observed higher improvement in the average power loss than that in the average system efficiency, again 24.5% versus 8.6%.

TABLE V
AVERAGE POWER LOSS AND TOTAL ENERGY LOSS.

	Con. design	Proposed design
P_{loss}^{avg}	3.55 W	2.68 W
E_{loss}	47073 J	35537 J

For reference purposes, an additional charging profile (solid line) and experimental/calculated results are shown in Fig. 13 and 14, respectively, when using a different type of battery cell (4S1P), TNL-ITR18650. The total charging time of the TNL-ITR18650 battery pack is 208 min and the pack voltage reaches its nominal value at 95 min. Due to the different charging profile, the design parameters are recalculated through the proposed design, $\mathbf{x}_{\mathbf{opt}}^{'}$=[126 pF, 240 pF, 180 pF, 262 pF, 110 pF] and $L_s^{'}$=328 nH. Similar improvements in the system efficiency and power loss are observed in Fig. 14(a) and (b). Table VI summarizes the average power loss in the conventional design and proposed design, P_{loss}^{avg}, when charging the two different battery packs. Applying the proposed design methodology, the average power loss during the entire charging cycle is significantly reduced by about 25% for the both battery packs.

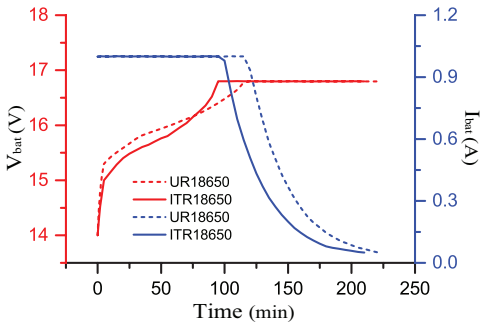

Fig. 13. Charging profiles of TNL-ITR18650 battery pack and SANYO UR18650 battery pack.

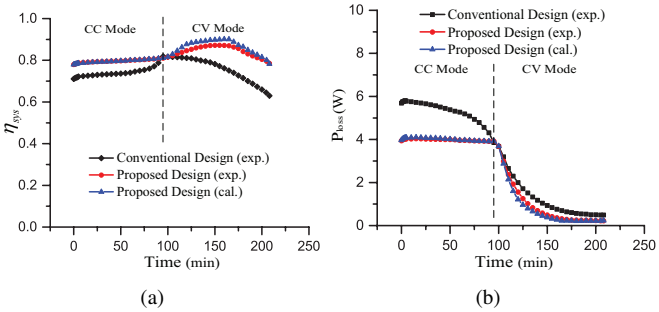

Fig. 14. Experimental results when charging TNL-ITR18650 battery pack. (a) system efficiency. (b) power loss.

TABLE VI
AVERAGE POWER LOSS WHEN CHARGING TWO BATTERY PACKS.

	UR18650	ITR18650
Con. design	3.55 W	3.36 W
Proposed design	2.68 W	2.46 W
Reduction	24.5%	26.8%

VI. CONCLUSIONS

This paper proposes a systematic design methodology for a high-efficiency 6.78-MHz Class E^2 wireless battery charging system. Through the preliminary analysis, it shows that the

non-neglectable and varying input reactance of the Class E rectifier adversely affects the efficiency of the system when following the battery charging profile. The average power loss is then defined based on the analytically derived system efficiency and discretized charging file. The design parameters, the five capacitors and one inductor, are optimized later that minimizes the average power loss during the entire battery charging cycle. The experiments show that the proposed design achieves a significant reduction of the average power loss, 24.5%, when comparing with that through the conventional design. The design methodology proposed in this paper is a general solution that enables high-efficiency MHz wireless charging under any specific battery charging profile.

REFERENCES

[1] A. P. Sample, B. H. Waters, S. T. Wisdom, and J. R. Smith, "Enabling seamless wireless power delivery in dynamic environments," *Proc. IEEE*, vol. 101, no. 6, pp. 1343–1358, Jun. 2013.

[2] S. Hui, W. Zhong, and C. Lee, "A critical review of recent progress in mid-range wireless power transfer," *IEEE Trans. Power Electron.*, vol. 29, no. 9, pp. 4500–4511, Sep. 2014.

[3] N. Keeling, G. Covic, J. T. Boys *et al.*, "A unity-power-factor IPT pickup for high-power applications," *IEEE Trans. Ind. Electron.*, vol. 57, no. 2, pp. 744–751, Feb. 2010.

[4] H. Li, K. W. Jie Li, W. Chen, and X. Yang, "A maximum efficiency point tracking control scheme for wireless power transfer systems using magnetic resonant coupling," *IEEE Trans. Power Electron.*, vol. 30, no. 7, pp. 3998–4008, Jul. 2015.

[5] S. Li, W. Li, J. Deng, T. D. Nguyen, and C. C. Mi, "A double-sided LCC compensation network and its tuning method for wireless power transfer," *IEEE Trans. Veh. Technol.*, vol. 64, no. 6, pp. 2261–2273, Jun. 2015.

[6] W. Zhong and S. Hui, "Maximum energy efficiency tracking for wireless power transfer systems," *IEEE Trans. on Power Electron.*, vol. 30, no. 7, pp. 4025–4034, Jul. 2015.

[7] M. Pinuela, D. C. Yates, S. Lucyszyn, and P. D. Mitcheson, "Maximizing DC-to-load efficiency for inductive power transfer," *IEEE Trans. Power Electron.*, vol. 28, no. 5, pp. 2437–2447, May. 2013.

[8] W. Zhong, C. Zhang, X. Liu, and S. Hui, "A methodology for making a three-coil wireless power transfer system more energy efficient than a two-coil counterpart for extended transfer distance," *IEEE Trans. Power Electron.*, vol. 30, no. 2, pp. 933–942, Feb. 2015.

[9] M. Fu, T. Zhang, C. Ma, and X. Zhu, "Efficiency and optimal loads analysis for multiple-receiver wireless power transfer systems," *IEEE Trans. Microw. Theory Tech.*, vol. 63, no. 3, pp. 801–812, Mar. 2015.

[10] N. Sokal and A. Sokal, "Class E-A new class of high-efficiency tuned single-ended switching power amplifiers," *IEEE J. Solid-State Circuits*, vol. 10, no. 3, pp. 168–176, Jun. 1975.

[11] W. Chen, R. Chinga, S. Yoshida, J. Lin, C. Chen, and W. Lo, "A 25.6 W 13.56 MHz wireless power transfer system with a 94% efficiency GaN Class-E power amplifier," in *IEEE MTT-S Int. Microw. Symp. Dig.*, pp. 1–3, Montreal, QC, Canada, Jun. 2012.

[12] S. Aldhaher, P.-K. Luk, A. Bati, and J. Whidborne, "Wireless power transfer using Class E inverter with saturable DC-feed inductor," *IEEE Trans. Ind. Appl.*, vol. 50, no. 4, pp. 2710–2718, Jul. 2014.

[13] S. Aldhaher, P.-K. Luk, and J. F. Whidborne, "Electronic tuning of misaligned coils in wireless power transfer systems," *IEEE Trans. Power Electron.*, vol. 29, no. 11, pp. 5975–5982, Nov. 2014.

[14] S. Liu, M. Liu, M. Fu, C. Ma, and X. Zhu, "A high-efficiency Class-E power amplifier with wide-range load in wpt systems," in *Proc. IEEE Wireless Power Transfer Conference (WPTC)*, Boulder, CO, USA, May. 2015.

[15] W. Nitz, W. Bowman, F. Dickens, F. Magalhaes, W. Strauss, W. Suiter, and N. Ziesse, "A new family of resonant rectifier circuits for high frequency DC-DC converter applications," in *Proc. Appl., Power Electron. Conf.*, pp. 12–22, New Orleans, LA, USA, Feb. 1988.

[16] S. Aldhaher, P.-K. Luk, K. El Khamlichi Drissi, and J. Whidborne, "High-input-voltage high-frequency Class E rectifiers for resonant inductive links," *IEEE Trans. Power Electron.*, vol. 30, no. 3, pp. 1328–1335, Mar. 2015.

[17] H. V. Venkatasetty and Y. U. Jeong, "Recent advances in lithium-ion and lithium-polymer batteries," in *Proc. The Seventeenth Annual Battery Conference on Applications and Advances*, pp. 173–178, Long Beach, CA, USA, Jan. 2002.

[18] A. Khaligh and Z. Li, "Battery, ultracapacitor, fuel cell, and hybrid energy storage systems for electric, hybrid electric, fuel cell, and plug-in hybrid electric vehicles: State of the art," *IEEE Trans. Veh. Technol*, vol. 59, no. 6, pp. 2806–2814, Jul. 2010.

[19] X. Qu, H. Han, S. C. Wong, C. K. Tse, and W. Chen, "Hybrid IPT topologies with constant current or constant voltage output for battery charging applications," *IEEE Trans. Power Electron.*, vol. 30, no. 11, pp. 6329–6337, Nov. 2015.

[20] P.-K. Luk, S. Aldhaher, W. Fei, and J. Whidborne, "State-space modeling of a Class E^2 converter for inductive links," *IEEE Trans. Power Electron.*, vol. 30, no. 6, pp. 3242–3251, Jun. 2015.

[21] M. Kazimierczuk, "Class E low dvd/dt rectifier," *Electric Power Applications, IEE Proceedings B*, vol. 136, no. 6, pp. 257–262, Nov. 1989.

[22] M. Albulet, *RF power amplifiers*. SciTech Publishing, 2001.

[23] M. Li, S. Azarm, and A. Boyars, "A new deterministic approach using sensitivity region measures for multi-objective robust and feasibility robust design optimization," *Journal of mechanical design*, vol. 128, no. 4, pp. 874–883, Dec. 2006.

[24] M. J. Neath, A. K. Swain, U. K. Madawala, and D. J. Thrimawithana, "An optimal PID controller for a bidirectional inductive power transfer system using multiobjective genetic algorithm," *IEEE Trans. Power Electron.*, vol. 29, no. 3, pp. 1523–1531, Mar. 2014.

[25] M. Fu, H. Yin, X. Zhu, and C. Ma, "Analysis and tracking of optimal load in wireless power transfer systems," *IEEE Trans. Power Electron.*, vol. 30, no. 7, pp. 3952–3963, Jul. 2015.

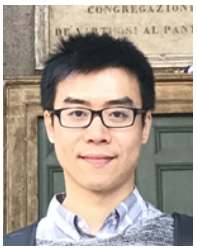

Ming Liu (S'15) received the B.S. degree from SiChuan University, Sichuan, China, in 2007, and the M.S. degree from the University of Science and Technology Beijing, Beijing, China, in 2011, both in mechatronic engineering. He is currently working toward the Ph.D. degree in electrical and computer engineering from the University of Michigan-Shanghai Jiao Tong University Joint Institute, Shanghai Jiao Tong University, Shanghai, China.

His research interests include high frequency power electronic circuits such as high frequency resonant converters and megahertz wireless power transfer systems, general power electronics and applications, circuit and system-level optimization.

Chen Zhao received the B.S. degree in electrical engineering and automation from East China University of Science and Technology, Shanghai, China, in 2011, and Ph.D. degree in electrical and computer engineering from University of Michigan-Shanghai Jiao Tong University Joint Institute, Shanghai Jiao Tong University, China, in 2016. He is currently a systems engineer with United Automotive Electronic Systems Co., Ltd, Shanghai, China.

His research interests include modeling and testing of lithium-ion batteries and control of battery-ultracapacitor hybrid energy storage systems.

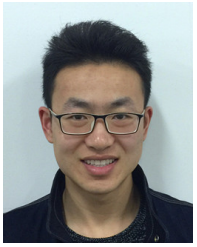

Jibin Song (S'16) received the B.S. degree in measurement & control technology and instrumentation from Jilin University, Jilin, China, in 2016. He is currently working toward the Ph.D. degree in electrical and computer engineering, University of Michigan-Shanghai Jiao Tong University Joint Institute, Shanghai Jiao Tong University, Shanghai, China.

His research interests include power electronics, design and optimization of multiple-receiver megahertz wireless power transfer systems.

Chengbin Ma (M'05) received the B.S. (Hons.) degree in industrial automation from East China University of Science and Technology, Shanghai, China, in 1997, and the M.S. and Ph.D. degrees both in electrical engineering from University of Tokyo, Japan, in 2001 and 2004, respectively. He is currently an associate professor of electrical and computer engineering with the University of Michigan-Shanghai Jiao Tong University Joint Institute, Shanghai Jiao Tong University, China. He is also with a joint faculty appointment in School of Mechanical Engineering, Shanghai Jiao Tong University. Between 2006 and 2008, he held a post-doctoral position with the Department of Mechanical and Aeronautical Engineering, University of California Davis, USA. From 2004 to 2006, he was a R&D researcher with Servo Laboratory, Fanuc Limited, Japan.

His research interests include wireless power transfer, networked hybrid energy systems such as microgrids and smart grids, and mechatronic control.